Predicting the effect of angular momentum on the dissociation dynamics of highly rotationally excited radical intermediates

Matthew D. Brynteson and Laurie J. Butler[a)]
Department of Chemistry and the James Franck Institute, The University of Chicago, Chicago, Illinois 60637, USA

(Received 2 July 2014; accepted 30 December 2014; published online 2 February 2015)

We present a model which accurately predicts the net speed distributions of products resulting from the unimolecular decomposition of rotationally excited radicals. The radicals are produced photolytically from a halogenated precursor under collision-free conditions so they are not in a thermal distribution of rotational states. The accuracy relies on the radical dissociating with negligible energetic barrier beyond the endoergicity. We test the model predictions using previous velocity map imaging and crossed laser-molecular beam scattering experiments that photolytically generated rotationally excited CD_2CD_2OH and C_3H_6OH radicals from brominated precursors; some of those radicals then undergo further dissociation to CD_2CD_2 + OH and C_3H_6 + OH, respectively. We model the rotational trajectories of these radicals, with high vibrational and rotational energy, first near their equilibrium geometry, and then by projecting each point during the rotation to the transition state (continuing the rotational dynamics at that geometry). This allows us to accurately predict the recoil velocity imparted in the subsequent dissociation of the radical by calculating the tangential velocities of the CD_2CD_2/C_3H_6 and OH fragments at the transition state. The model also gives a prediction for the distribution of angles between the dissociation fragments' velocity vectors and the initial radical's velocity vector. These results are used to generate fits to the previously measured time-of-flight distributions of the dissociation fragments; the fits are excellent. The results demonstrate the importance of considering the precession of the angular velocity vector for a rotating radical. We also show that if the initial angular momentum of the rotating radical lies nearly parallel to a principal axis, the very narrow range of tangential velocities predicted by this model must be convoluted with a J = 0 recoil velocity distribution to achieve a good result. The model relies on measuring the kinetic energy release when the halogenated precursor is photodissociated via a repulsive excited state but does not include any adjustable parameters. Even when different conformers of the photolytic precursor are populated, weighting the prediction by a thermal conformer population gives an accurate prediction for the relative velocity vectors of the fragments from the highly rotationally excited radical intermediates. © *2015 AIP Publishing LLC.* [http://dx.doi.org/10.1063/1.4905776]

I. INTRODUCTION

Studying the gas-phase unimolecular decomposition of radicals is important in better understanding combustion, atmospheric chemistry, decomposition of energetic materials, and the chemistry occurring in interstellar space. Two definitive methods to study the unimolecular dissociation dynamics of radicals use collision-free conditions to isolate the chemistry of these highly reactive intermediates, velocity map imaging (VMI), and crossed laser-molecular beam scattering measurements. In these experiments, radicals are generated from the photolysis of a halogenated precursor and the internal energy distribution in the nascent radicals is determined by measuring the energy partitioned to recoil kinetic energy, detecting the momentum-matched halogen co-fragment. Depending on the internal energy imparted to these radicals, the radicals may remain stable to further dissociation, or they may have sufficient vibrational energy to undergo various isomerizations and dissociations.[1–7] The dissociation dynamics of the unstable radicals are detected by measuring the velocity distribution of the resulting products. The unimolecular dissociation rate of the radical intermediates, as well as the product branching, may be influenced by the partitioning of its internal energy between vibrational and rotational energy. In statistical calculations of these unimolecular dissociation rates, it is often assumed that the rotational energy at the transition state is well represented by a thermal distribution, but this is not the case when the radical is produced photolytically and under collision-free conditions.

Previous efforts to better understand energy partitioning resulting from photodissociation have made the use of impulsive dissociation models when the photolytic precursor is promoted to an excited electronic state that is strongly repulsive in the Franck-Condon region. Such models have been used to estimate the translational and rotational energy imparted to the photofragments with varying levels of success.[8–13] Overall, however, the estimate of the translational energy imparted to the photofragments only qualitatively

a)Author to whom correspondence should be addressed. Electronic mail: l-butler@uchicago.edu

agrees with the experimental results. Our approach[14–16] instead uses the measured recoil kinetic energy distribution, using an impulsive model only to determine the partitioning of energy to rotational energy in the radicals at each measured recoil velocity between the halogen atom co-fragment and the radical.

Our method begins by using the experimentally determined speeds of the primary halogen photofragment to calculate the angular momentum of the recoiling radical intermediates. Rather than using an impulsive dissociation model to estimate both the translational and rotational energy of the radicals, the measurement of the halogen co-fragment speed distribution determines the magnitude of the linear momentum, $|\mu\vec{v}_{rel}|$, imparted to the fragments upon photodissociation. An impulsive approximation is used only to define the angle between $\vec{v}_{rel}$ and the vector between the center of mass of the radical moiety and the halogen co-fragment. We assume the impulsive force is directed along the bond from the halogen atom to the atom in the radical moiety to which it is bonded, using the geometry of the precursor prior to photo-excitation (the Franck-Condon region). The distribution of angular momentum vectors of the nascent radical is then easily calculated from this geometry and the measured $|\mu\vec{v}_{rel}|$. This impulsive dissociation model for the J distribution of the nascent radicals may then be used to predict the portion of the radicals' speed distribution that is stable to subsequent dissociation (having insufficient vibrational energy to surmount any dissociation or isomerization barrier). The best predictions result when we correct for the change in rotational energy of the radical, $E_{rot} = \frac{1}{2}\mathbf{J}^T\mathbf{I}^{-1}\mathbf{J}$, as the radical changes geometry *en route* to each transition state. We have used the photodissociation of brominated precursors at 193 nm, $BrCD_2CD_2OH$[16] and BrC_3H_6OH (*vide infra*), to test the accuracy of the prediction for the angular momentum imparted to the radicals; the results are excellent provided the relative speeds between the radical and the halogen co-fragment from the precursor photodissociation are empirically determined.

The radical species generated in these experiments often have sufficient vibrational energy to undergo subsequent unimolecular dissociation. The net recoil velocity of the products when the radical dissociates is the vector sum of the initial velocity of the radical and the velocity imparted to each product when the radical dissociates. Our new method avoids a common assumption made in fitting the net speed distributions measured in VMI experiments (or the neutral fragment time-of-flight (TOF) spectra in scattering experiments) of the radicals' dissociation fragments. Typically it is assumed that the distribution of recoil kinetic energies imparted in the secondary dissociation of the radical is independent of the velocity of the radical, so the same distribution of recoil kinetic energies imparted in the second step may be used for all the radical intermediates. That is, the primary speeds of the unstable radicals are convolved[17–19] over the entire range of secondary speeds of the dissociation fragments; no correlation is assumed. However, for rotationally excited radicals having sufficient vibrational energy to dissociate, their unimolecular decomposition results in fragments with significant relative velocities due to the tangential velocities of the rotating radicals during dissociation. This effect can lead to a strong correlation between the radical's velocity vector and the corresponding relative velocity vector of its decomposition products. In most prior studies involving the dissociation of rotationally excited radicals, this correlation is ignored.

A correlation between the speeds of the radical and the dissociation fragments was considered by Hintsa *et al.*[20] in a study of the photodissociation of 2-bromoethanol and 2-chloroethanol at 193 nm. They noted that using a single secondary $P(E_T)$ for the dissociation of the β-hydroxyethyl radicals could not fit all dissociation fragments (OH and ethene) simultaneously. Therefore, they used a secondary $P(E_T)$ of the form shown by Eq. (1), which is related to statistical theory of unimolecular dissociation. In Eq. (1), E_T is the relative translational energy between the OH and ethene fragments, a is a normalization constant, b is the expected barrier height, E_{tot} is the total internal energy of the radical, r is the dimensionality of the reaction coordinate, and w is the number of active modes. The best fit to their data was obtained with $b = 6$, $r = 1$, and $w = 1.5$. However, while Hintsa *et al.* noted this correlation between the primary and secondary $P(E_T)$s, the dependence was simply related to the excess energy above the barrier rather than the radicals' rotational energy,

$$P(E_T) = a(E_T - b)^r (E_{tot} - E_T)^w. \quad (1)$$

As mentioned, our recent studies on the photodissociation of 2-bromoethanol and 2-bromoethanol-d_4 at 193 nm have made use of the experimentally-measured bromine speed distributions to calculate the angular momenta imparted to the radicals upon photodissociation. The resulting angular momenta were used to predict the portions of the total $P(E_T)$ corresponding to stable and unstable radicals, which agreed quite well with the experimentally measured speeds of the stable radicals. In these experiments, an unexpectedly high branching to the vinyl + H_2O channel was observed[21,22] in comparison to the expected branching to OH + ethene (the lowest barrier dissociation channel). The vinyl + H_2O channel was proposed to occur via a "frustrated" dissociation or "roaming" pathway by Kamarchik *et al.*[23] who performed quasiclassical trajectory calculations on vibrationally excited β-hydroxyethyl radicals. Womack *et al.*[22] proposed that the unexpected branching to vinyl + H_2O may be the result of the change in inertial tensor *en route* to the transition state. This inertial change has the effect of decreasing the energy difference between the respective OH and H_2O loss transition states as the rotational energy increases, and as the radicals in those experiments were highly rotationally excited, that may be an explanation for the higher-than-expected branching to vinyl + H_2O.

To further investigate the effects of rotational energy on the dissociation of β-hydroxyethyl radicals, McKown *et al.*[24] performed quasi-classical trajectory calculations on these radicals. In those trajectory calculations, the initial conditions given to the radicals were set to mimic the angular momenta of the radicals generated in the photolysis experiment. While the results did not yield the expected branching to the vinyl + H_2O channel, they did demonstrate a strong angular momentum dependence

of the relative speeds between the OH + ethene fragments upon unimolecular dissociation of the β-hydroxyethyl radicals. The marked difference between the predicted OH + ethene $P(E_T)$s for J = 0 and J = 127 a.u. β-hydroxyethyl radicals underscores the necessity to include a correlation between the radicals' velocity vectors and the dissociation fragments' velocity vectors in fitting the experimentally-measured net speed distributions or TOF spectra.

This work presents a new model which predicts the velocities imparted to the fragments upon dissociation of three different rotationally excited radicals: (1) β-hydroxyethyl-d_4 radicals, (2) 1-hydroxy-2-propyl radicals, and (3) 2-hydroxy-1-propyl radicals as shown in Eqs. (2)–(4),

$$CD_2CD_2OH \rightarrow CD_2CD_2 + OH, \quad (2)$$

$$CH_2(OH)CHCH_3 \rightarrow C_3H_6 + OH, \quad (3)$$

$$CH_2C(OH)HCH_3 \rightarrow C_3H_6 + OH. \quad (4)$$

The ground electronic state dissociation of each of these radicals was studied in prior work[16,22] on the photodissociation of 2-bromoethanol-d_4 and a 70/30 mixture of 1-bromo-2-propanol and 2-bromo-1-propanol at 193 nm. High-level calculations[25–35] of the minima and transition states on the potential energy surfaces for these radicals show that the dissociation to OH + ethene-d_4 (from the β-hydroxyethyl-d_4 radicals) or OH + propene (from the 1-hydroxy-2-propyl and 2-hydroxy-1-propyl radicals) proceeds via a transition state with no barrier beyond the endoergicity. As a result, we expect to be able to calculate the relative velocities of the OH + ethene-d_4 and OH + propene fragments by determining the tangential rotational velocity of each fragment during the dissociation of the given radical. We then use the results of our model to predict the net speed distribution of each fragment, and these net speed distributions are used to fit the experimentally measured TOF spectra. We describe these calculations in detail here and provide the code for applying this methodology to other systems in the supplementary material.[36] We trust they will be useful for those fitting similar data to that analyzed here. More generally, we note that any statistical treatment of unimolecular dissociation rates relies on dividing the energy at the transition state between rotation and vibration; when the system being studied is a radical produced photolytically, the analysis presented here demonstrates the situations under which one can estimate this rotational energy accurately and predict the resulting dissociation dynamics of the radical.

II. METHODS

Before discussing the details of the model employed in this work, we give a very brief explanation of the experiments to be modelled. The dissociation of rotationally excited CD_2CD_2OH and C_3H_6OH radicals has been previously studied using a crossed laser-molecular beam TOF scattering apparatus. In these experiments, a brominated photolytic precursor to the radicals was seeded in an inert gas (typically He or Ne) and supersonically expanded through a continuous or pulsed valve into a very low pressure environment ($<10^{-5}$ Torr). This expansion is then collimated by one or two skimmers, creating a molecular beam. The molecular beam is then intersected with a photolysis laser (193 nm for the case of the experiments modeled herein) which excites the molecules to an excited state repulsive in the C–Br bond. Prompt photolytic cleavage of the C–Br bond generates the radicals of interest. The unstable radicals are imparted rotational and vibrational energies in this process, and undergo unimolecular dissociation. The velocities of the primary Br photofragments and the products of the momentum-matched radicals that dissociate are then detected in a crossed laser-molecular beam scattering apparatus. Neutral product TOF spectra, with the flight path being from the interaction region between the laser and molecular beam to the ionization region in the detector, are obtained for each species. The method presented herein models the dissociation of rotationally excited radicals and predicts the recoil velocities (speeds and direction with respect to the initial velocity of the unstable radical produced from C–Br photofission in the precursor) of the dissociation products. The predicted velocity distributions are then used to generate fits to the TOF spectra obtained in the experimental work. Further details on these experiments can be found in Refs. 16 and 22.

We calculate the angular momenta of the recoiling radical intermediates produced from C–Br photofission by employing an impulsive model described previously.[14–16,37] Briefly, we assume the total angular momentum is zero prior to photodissociation and neglect the angular momentum of the photon and any electronic angular momenta. Upon photolysis, the rotational angular momentum of the recoiling radical intermediate is equal in magnitude and opposite in direction to the orbital angular momentum of the recoiling halogen and the momentum-matched radical. The orbital angular momentum is found by $\vec{J}_{orb} = \vec{r} \times \vec{P}_{rel}$, where $\vec{r}$ is the vector between the centers of mass of the radical moiety in the precursor and the halogen as determined using the precursors' equilibrium geometries in the ground electronic state. $\vec{P}_{rel}$ is the linear recoil momentum, $\mu \vec{v}_{rel}$, taken as along the carbon-halogen bond; the magnitude is determined from the experimentally measured speed distribution of the halogen. The rotational angular momentum of the recoiling radical is then $\vec{J}_{radical} = -\vec{J}_{orb}$.

If the resulting rotational motion is about a principal axis of the radical moiety, then $\vec{J} = I\vec{\omega}$ where I is a scalar moment of inertia. More generally, $\vec{J}$ is not along a principal axis, so the tensor of inertia $\boldsymbol{I}$ is used in our model. Then, of course, $\vec{\omega}$ precesses about $\vec{J}$ and tumbles as the tensor, $\boldsymbol{I}$, changes during the rotation. We model the dynamics by keeping the angular momentum fixed in space as required by the conservation of angular momentum.

By mapping $\vec{J}_{radical}$ onto the radical's equilibrium geometry, the instantaneous angular velocity vector, $\vec{\omega}$, is found by $\vec{\omega} = \boldsymbol{I}^{-1}\vec{J}_{radical}$, where $\boldsymbol{I}^{-1}$ is the inverse of the tensor of inertia of the radical. We then model the rotation of the radical by allowing it to undergo a very small rotation, $\Delta\theta_\omega$, about the instantaneous angular velocity vector. After this small rotation, $\Delta\theta_\omega$, the tensor of inertia is recalculated, which results in a new instantaneous angular velocity vector. This procedure is carried out to allow the radical to undergo

any number of rotations. Section XII in the supplementary material[36] gives a sample plot demonstrating the precession of $\vec{\omega}$ about $\vec{J}_{radical}$ by plotting the angle between the two vectors as a function of the number of rotations for the CD_2CD_2OH radical which results from the photodissociation of the Gg conformer of 2-bromoethanol-d_4. The trajectory results using $\Delta\theta_\omega = 0.001$ and 0.0001 radians show consistent results even up to 30 rotations. Therefore, we use $\Delta\theta_\omega = 0.0001$ radians for trajectories involving the rotation of the radicals at their stationary point geometries. The advantages gained by further decreasing $\Delta\theta_\omega$ are offset by the disadvantage of requiring more trajectory points to obtain the same number of rotations.

We then model the tangential velocity imparted to the fragments resulting from dissociation of the rotationally excited radicals. For dissociations without a barrier beyond the endoergicity, such as those modelled in this work, the relative velocity between the dissociation fragments should simply result from the tangential velocity during the rotation as no additional substantial forces are expected between the two fragments after the transition state. Additionally, we neglect any bending motions in the dissociating radicals. A discussion of the bending motions which may impart additional relative velocity to the dissociating fragments is found in Sec. III D. To model the dissociation event, the geometry of the rotating radical is changed from that at the stationary point geometry to that at a pre-chosen transition state geometry using the properly weighted normal mode displacement vectors and fixing $\vec{J}_{radical}$ in space (the direction and magnitude of $\vec{J}_{radical}$ are conserved). After this change in geometry, we follow the successive rotations at the transition state. This process occurs at each trajectory point over a chosen range of radical rotations that samples the full range of angles between the precessing angular velocity vector and $\vec{J}_{radical}$. As this process is repeated, we choose $\Delta\theta_\omega = 0.001$ radians rather than 0.0001 radians for the transition state rotations as the results do not differ significantly for total rotations greater than 20. By 20 rotations, the simulations give very similar results; a comparison showing the results for 20 and 30 transition state rotations is given in the supplementary material.[36] The converged results, at approximately 20 transition state rotations, give the resulting speed distribution predictions that agree very well with the experimental data. We present those results in the text; the results using a smaller number of TS rotations (3, 10, and 15) are provided in the supplementary material.[36]

The tangential velocity of the two fragments resulting from the dissociating radicals is then calculated at each transition state trajectory point using $\vec{v}_T = \vec{\omega} \times \vec{r}$, where $\vec{v}_T$ is the tangential velocity of one of the departing fragments, $\vec{\omega}$ is the angular velocity vector at that trajectory point, and $\vec{r}$ is the vector between the center of mass of the radical and the center of mass of the departing fragment. In this manner, the tangential velocity of each of the two recoil fragments is determined, and their relative translational energy is calculated as $E_T'' = \frac{1}{2}\mu'' v_{rel}''^2$, where μ'' is the reduced mass of the two recoiling fragments and v_{rel}'' is the magnitude of the relative velocity vector between the fragments. We have added the double prime here to distinguish between the secondary dissociation of the radical (double prime) and the primary C–Br photolysis (single prime). The ratio of the fragments' relative translational energy, E_T'', to the relative translational energy of the radical and the halogen, E_T', is stored at each trajectory point and used to generate the distribution $P\left(\frac{E_T''}{E_T'}\right)$ resulting from the precession of the angular velocity vector. Also stored at each trajectory point is the angle, $\theta_{v_R', v''}$, between the velocity vector of the radical, $\vec{v}_R'$, imparted in the C–Br photolysis and the tangential velocity vector for one of the two fragments from the dissociation of the radical, $\vec{v}''$, which is used to generate the angular distribution $I\left(\theta_{v_R', v''}\right)$.

The $P(E_T')s$ of the unstable radicals, as determined using the method in Ref. 16, are then used in combination with the $P\left(\frac{E_T''}{E_T'}\right)$ and the $I\left(\theta_{v_R', v''}\right)$ trajectory results to derive the net speed (v_{net}) distributions of the unimolecular dissociation products. At each value of E_T', the corresponding range of E_T'' values are determined using the $P\left(\frac{E_T''}{E_T'}\right)$. The resulting radical speed v_R' and range of dissociation fragment speeds, v'', are then convolved over $I\left(\theta_{v_R', v''}\right)$, to determine the net speeds and corresponding probabilities. This process results in the net speed distributions of the dissociation fragments. Because each halogenated precursor has multiple conformers, the net speed distributions for the dissociation of each conformer are determined, weighted by the expected contribution from each conformer, and summed together to yield the total net speed distribution. The expected contribution from each conformer is determined by the calculated thermal conformer populations of the photolytic precursor,[15,16] weighted by the predicted percentages of unstable radicals resulting from each conformer.

These results are then used to generate fits to previously experimentally[16,22] obtained TOF spectra for the unimolecular dissociation fragments of the radical. The TOF spectra of the OH and ethene-d_4/propene fragments were experimentally determined using a crossed laser-molecular beam apparatus in which the radicals were generated via 193 nm photolysis of brominated precursors. These experiments were performed at the National Synchrotron Radiation Research Center (NSRRC) in Hsinchu, Taiwan. Further information regarding the experimental details can be found in Refs. 16 and 22. Using the trajectories for rotating CD_2CD_2OH and C_3H_6OH radicals resulting from the 193 nm photodissociation of 2-bromoethanol-d_4 and a 70/30 mixture of 1-bromo-2-propanol and 2-bromo-1-propanol, we use the above methods to predict the speed distributions of the fragments resulting from the OH-loss unimolecular dissociation channels.

III. RESULTS

A. OH + CD_2CD_2 / C_3H_6OH systems

Using the trajectory calculations described in Sec. II, the dissociation dynamics of three rotationally-excited radicals were investigated. Those radicals are the β-hydroxyethyl-d_4 radical (CD_2CD_2OH), the 2-hydroxy-1-propyl radical ($CH_3CH(OH)CH_2$), and the 1-hydroxy-2-propyl radical ($CH_3CHCH_2(OH)$). The dissociations of each of these three radicals to OH and the respective ethene-d_4 or propene

cofragments proceed via a ~26 kcal/mol transition state barrier (through a minor van der Waals complex) with approximately no barrier beyond the endoergicity.[25–35] Consequently, the relative speeds of the dissociation fragments should result only from the tangential velocity experienced during the dissociation (if one neglects any velocity component due to vibrational motion of the radical).

The measured recoil velocity distribution of the Br atoms together with the assumption of an impulsive dissociation at the precursor geometry was employed to determine the angular momentum imparted to the radicals during the dissociation process. This was then used to predict the portion of radicals having vibrational energy below the dissociation barrier to OH + ethene-d_4/propene adjusted for the rotational energy, $E_{rot} = \frac{1}{2}\vec{J}^T \boldsymbol{I}^{-1}\vec{J}$, using the different tensors of inertia at the transition state. These predictions agreed quite well with the measured speed distributions of the stable radicals, supporting the method used to determine the angular momentum. The portions of the total, measured C–Br relative translational energy distributions, $P(E_T')$, resulting in unstable radicals are used in this work to derive the recoil velocity of the dissociating radicals.

Furthermore, the photolytic, brominated precursors have a variety of different conformers (5 for 2-bromoethanol, 8 for 2-bromo-1-propanol, and 9 for 1-bromo-2-propanol), all of which are discussed in detail in prior work.[15,16] The photodissociation of each conformer results in radicals with different angular momenta. However, many of the conformers differ only in the position of the hydrogen on the hydroxyl group, and therefore they do not have significantly different tensors of inertia. The conformers can then be collected into groups where the geometries found in each group differ only in the position of the hydrogen on the hydroxyl group. This reduction results in two groups for 2-bromoethanol, three groups for 1-bromo-2-propanol, and three groups for 2-bromo-1-propanol. The trajectories are run for each group, and the results are weighted by the expected OH + ethene-d_4 (or propene) contributions from each group and summed together.

For the dissociation of CD_2CD_2OH or C_3H_6OH to OH + ethene and OH + propene, respectively, different levels of theory calculate transition state geometries with varying C–O bond lengths. When considering the $C_3H_6OH \rightarrow$ OH + propene reaction, for example, Zador *et al.*[32] calculated the OH-addition transition states for both terminal and center-carbon addition at both the MP2/6-311++G(d,p) and CASPT2(3e,3o)/aug-VDZ levels of theory. Those methods resulted in transition state geometries with C–O bond lengths of 2.07 Å and 2.39 Å, respectively. The tensor of inertia at the transition state geometry affects the tangential velocity of the resulting fragments, and to consider this effect, we performed the trajectory calculations using three different transition state geometries having C–O bond lengths given in Table I. The geometries of transition states with short C–O bond lengths (2.12 and 2.07 Å) and medium C–O bond lengths (2.4 and 2.34 Å) were calculated at the MP2/6-311++G(3df,2p) and B3LYP/6-311++G(3df,2p) levels of theory, respectively. The transition state geometries with long C–O bond lengths (2.58 Å) were generated by manually extending the C–O bond length and holding it fixed while optimizing the geometry in the orthogonal vibrational degrees of freedom. We present the trajectory results from each transition state geometry in the supplementary material.[36] Here in the text, we present the results which use the medium C–O bond length transition states as they best agree with the experimental data.

TABLE I. Transition state C–O bond distances.

$CD_2CD_2OH \rightarrow CD_2CD_2$+OH TS C–O bond distance (Å)	$C_3H_6OH \rightarrow C_3H_6$ + OH TS C–O bond distance (Å)
2.12	2.07
2.40	2.34
2.58[a]	2.58

[a]The 2.58 Å C–O bond length transition states were determined by manually extending the C–O bond length and minimizing the geometry in the other degrees of freedom.

As mentioned in Sec. II, the $P\left(\frac{E_T''}{E_T'}\right)$s and the $I\left(\theta_{v_R',v''}\right)$s for each group of conformers are determined by calculating the velocity vector for the center of mass of each product moiety at each point during the rotation of the transition state. Here in the text, we present the set yielding the best results: 20 transition state rotations at the medium C–O length (2.34 and 2.4 Å) transition state geometry. The average $\frac{E_T''}{E_T'}$ and E_T'' for all sets (different C–O bond length TS and number of TS rotations) are presented in Tables S10 and S2 in the supplementary material.[36]

B. Dissociation of the β-hydroxyethyl-d_4 radicals to OH + CD_2CD_2

2-Bromoethanol-d_4 has five conformers: Gg, Gg′, Gt, Tg, and Tt, where the first letter represents the *gauche* (G) or *trans* (T) relationship between the bromine and the hydroxyl group and the second letter represents the *gauche* (g) or *trans* (t) relationship between the hydroxyl's hydrogen and CH_2Br group. Because the hydrogen on the hydroxyl group has very little effect on the tensor of inertia of the CD_2CD_2OH moiety in 2-bromoethanol-d_4, we consider only the two groups having either a *gauche* (G) or *trans* (T) relationship between the bromine and the hydroxyl group.

Using the method described in Ref. 16, the percentages of stable and unstable radicals resulting from the dissociation of each group of conformers are calculated, and the speeds of the unstable β-hydroxyethyl-d_4 radicals are derived from the predictions of the unstable portions of the total C–Br fission $P(E_T')$. The portion of the measured C–Br $P(E_T')$'s that results in unstable CD_2CD_2OH and CD_2CD_2OH radicals from both the G and T 2-bromoethanol-d_4 precursor conformer groups are given in the top frame of Figure 1, and the calculated percentages of unstable radicals resulting from each conformer group are given in Table III.

The lower frame in Figure 1 presents the $P\left(\frac{E_T''}{E_T'}\right)$s resulting from our model trajectories for the dissociating CD_2CD_2OH radicals from both the G conformer group and T conformer group using the C–O bond length = 2.4 Å transition state and 20 transition state rotations. The $P\left(\frac{E_T''}{E_T'}\right)$ and $I\left(\theta_{v_R',v''}\right)$ results for all transition state geometries and

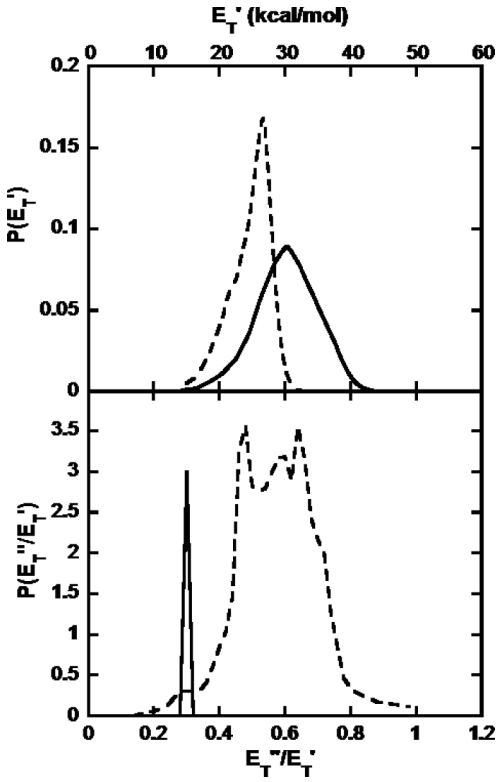

FIG. 1. (Top frame) Unstable portions of the measured C–Br P(E_T)s for the photodissociation of the G (dashed black distribution) and T (solid black distribution) conformer groups of 2-bromoethanol-d_4. (Lower frame) $P\left(\frac{E_T''}{E_T'}\right)$s for the dissociation of the CD_2CD_2OH radicals from the G conformer group (dashed black distribution) and CD_2CD_2OH radicals from the T conformer group (solid black distribution).

transition state rotations are supplied in the supplementary material.[36] The average $\frac{E_T''}{E_T'}$ values for each distribution are given in Table II. Immediately noticeable are the drastic differences between the $P\left(\frac{E_T''}{E_T'}\right)$s for the dissociation of the CD_2CD_2OH radicals from the G conformer group and CD_2CD_2OH radicals from the T conformer group. The differences result from the precession of the angular velocity vector about the angular momentum vector during rotation. The CD_2CD_2OH radicals from the T conformer group are

TABLE II. $\left\langle\frac{E_T''}{E_T'}\right\rangle$s and $\langle E_T''\rangle$s.

Conformer group[b]	$\left\langle\frac{E_T''}{E_T'}\right\rangle$	$\langle E_T''\rangle$ (kcal/mol)
G	0.58	13.7
T	0.30	8.6
2GG′	0.22	6.1
2TG	0.11	3.0
2G′T	0.07	1.7
1TG	0.42	11.5
1G′T	0.24	6.2

[a]The average $\frac{E_T''}{E_T'}$s and E_T''s reported in the table result from the trajectories using the 2.4 Å C–O length TS for the dissociation of CD_2CD_2OH radicals and the 2.34 Å C–O length TS for the dissociation of C_3H_6OH radicals.

[b]The first two conformer groups (G and T) are conformers of 2-bromoethanol-d_4 and the next five are conformer groups of 2-bromo-1-propanol and 1-bromo-2-propanol.

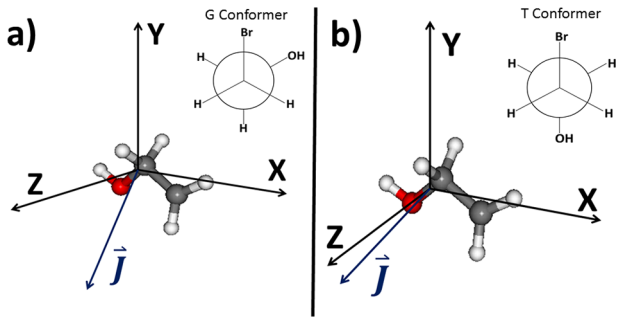

FIG. 2. Diagram demonstrating the instantaneous spatial relationship (for a single trajectory step) between the angular momentum vector ($\vec{J}$) and the principal axes (x, y, and z) of the rotating CD_2CD_2OH radicals resulting from photodissociation of the G conformer (left) and T conformer (right) of 2-bromoethanol-d_4. The angular momentum vector of the CD_2CD_2OH radicals resulting from photodissociation of the G conformer of 2-bromoethanol-d_4 points in a direction that is not close to any of the three principal axes, resulting in a large precession during the radical's rotation. In contrast, the angular momentum vector of the CD_2CD_2OH radicals resulting from the photodissociation of the T conformer of 2-bromoethanol-d_4 points in a direction closely aligned with one of the radical's principal axes, resulting in very little precession during rotation. The diagrams are taken from a single trajectory point during the total rotational trajectory calculation for each radical. The unit vectors in the direction of the principal axes and angular momenta are given in the supplementary material[36] for both (a) and (b).

imparted with an angular momentum, $\vec{J}$, that is very close to a principal inertial axis of the radical at its equilibrium geometry. This results in a very narrow $P\left(\frac{E_T''}{E_T'}\right)$ distribution and a correspondingly narrow range of tangential velocities of the OH and CD_2CD_2 upon dissociation. The angular momentum vector imparted to the CD_2CD_2OH radicals upon photodissociation of the G conformer group, however, differs significantly from all of the principal axes, resulting in a large precession of the angular velocity vector and, hence, a large range of tangential velocities of the OH and CD_2CD_2 fragments. This relationship of the angular momentum vector to the principal axes is depicted in Figure 2 which shows the instantaneous positions of the principal axes with respect to the angular momentum vector at one point during the trajectory. Figure 3 shows the plots of the angle, $\theta_{J,\omega}$, between the angular momentum vector and the angular velocity vector as a function of the number of rotations for both the CD_2CD_2OH radicals from the G conformer group and CD_2CD_2OH radicals from the T conformer group.

Convolving the unstable portions of the C–Br $P(E_T')$ over the $P\left(\frac{E_T''}{E_T'}\right)$s yields the predicted $P(E_T'')$s for the dissociation of the CD_2CD_2OH radicals to $OH + CD_2CD_2$ resulting from each conformer group. The results are shown in Figure 4. The $P(E_T'')$s for the dissociation of the CD_2CD_2OH radicals from the G and T conformer groups have $\langle E_T''\rangle$s of 14.3 kcal/mol and 8.6 kcal/mol, respectively. Furthermore, using the predicted unstable portions of the C–Br $P(E_T')$ and both the $P\left(\frac{E_T''}{E_T'}\right)$ and $I\left(\theta_{v'_R,v''}\right)$ the net speed distributions, $P(v_{net})$, of the OH and CD_2CD_2 fragments were developed as described in Sec. II. The results for net speed distribution predictions for the dissociation of CD_2CD_2OH radicals from each conformer group are shown in Figure 5 for the OH and ethene-d_4 fragments, respectively.

TABLE III. Contributions to the OH + CD_2CD_2/C_3H_6 channel from each conformer group.

Conformer group[a]	%unstable radicals[b]	Expected OH + CD_2CD_2 or OH + C_3H_6 contribution[c] (%)	Actual OH + CD_2CD_2 or OH + C_3H_6 contribution[d] (%)
T	87	55	55
G	21	45	45
1TG	65	13	15
1GG′	7	2	0
1G′T	55	45	50
2GG′	78	10	10
2TG	97	8	10
2G′T	98	22	15

[a]The first two conformer groups (G and T) are conformers of 2-bromoethanol-d_4 and the next six are conformer groups of 2-bromo-1-propanol and 1-bromo-2-propanol.
[b]The percentage of unstable radicals is calculated as the fraction of nascent radicals having vibrational energy above the centrifugally corrected dissociation barrier as discussed in Ref. 16.
[c]The expected contribution is determined by further weighting the percentage of unstable radicals from each conformer group by the relative population of each conformer group.
[d]The actual weightings are those used to obtain the best fit to the TOF spectra.

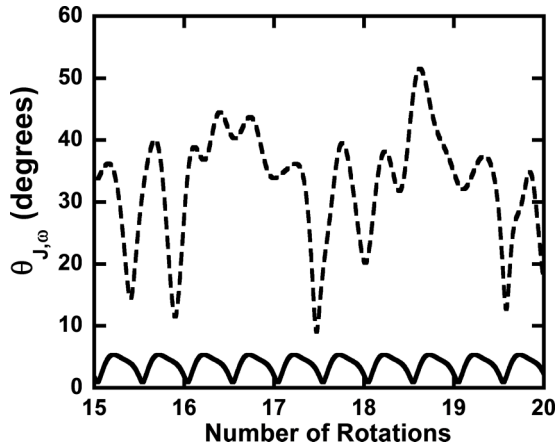

FIG. 3. $\theta_{J,\omega}$, the angle between the angular momentum vector and angular velocity vector, as a function of the number of rotations of the CD_2CD_2OH radicals from the G conformer group (dashed black line) and CD_2CD_2OH radicals from the T conformer group (solid black line). One rotation is defined as the number of trajectory points such that $\sum \Delta\theta_\omega = 2\pi$. The results displayed are at the equilibrium geometry of each radical; similar calculations are done at each transition state.

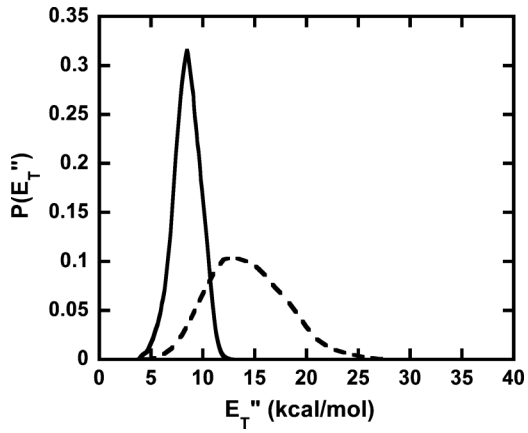

FIG. 4. $P(E_T'')$s for OH + CD_2CD_2 resulting from the dissociation of CD_2CD_2OH radicals from the G conformer group (dashed black distribution) and CD_2CD_2OH radicals from the T conformer group (solid black distribution).

Figure 6 shows the total net speed distributions predicted for both the OH and CD_2CD_2 fragments after weighting the contributions from each conformer group and summing them together. The total net speed distributions are used to generate fits to the TOF spectra for both the m/z = 32 ($CD_2CD_2^+$) and m/z = 17 (OH^+) TOF spectra measured in

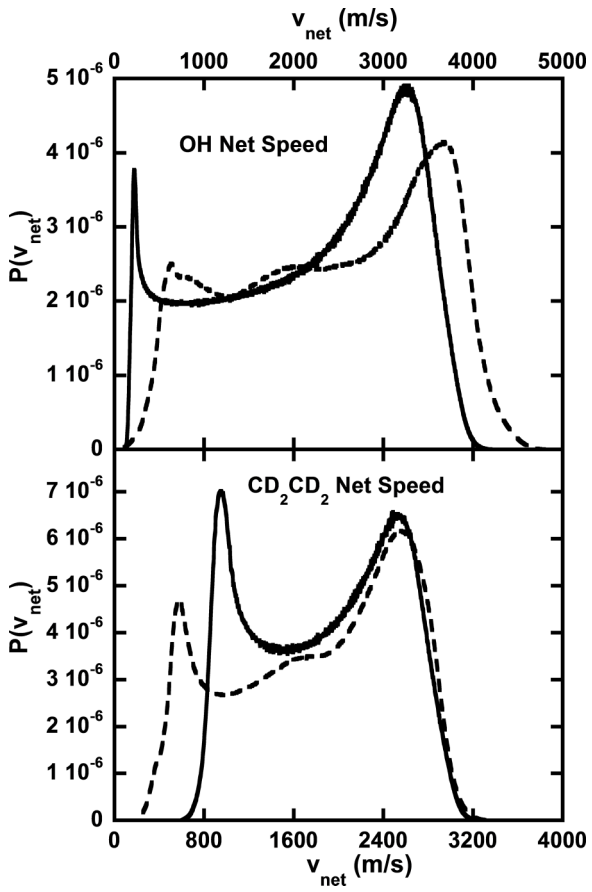

FIG. 5. $P(v_{net})$s for the OH (top frame) and CD_2CD_2 (lower frame) fragments resulting from the dissociation of CD_2CD_2OH radicals from the G conform group (dashed black distribution) and CD_2CD_2OH radicals from the T conformer group (solid black distribution).

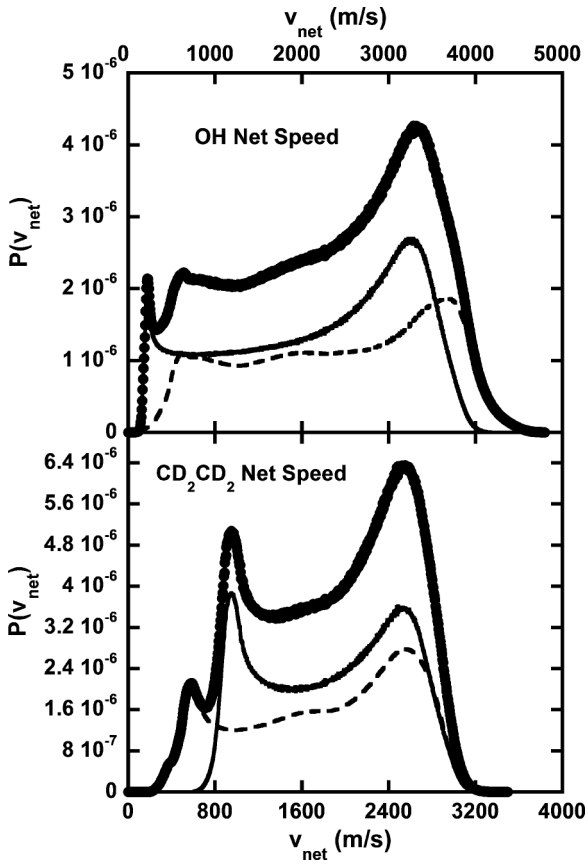

FIG. 6. Total $P(v_{net})$s (black bold line) for the OH fragments (top frame) and CD_2CD_2 fragments (lower frame) resulting from the dissociation of CD_2CD_2OH radicals from the G conformer group (dashed black distribution) and CD_2CD_2OH radicals from the T conformer group (solid black distribution) weighted by 45% and 55%, respectively.

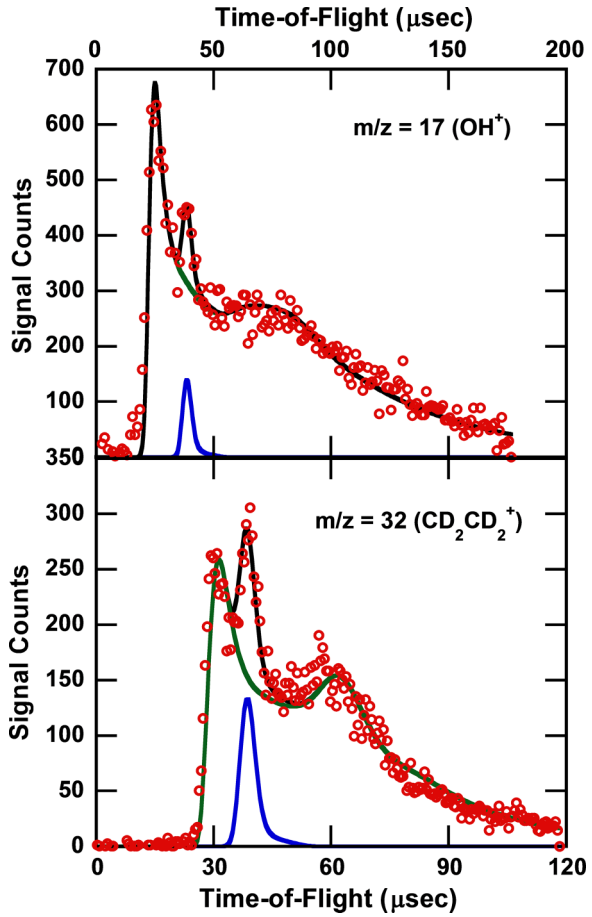

FIG. 7. TOF spectra for m/z = 17 (OH^+) (top frame) and m/z = 32 ($CD_2CD_2^+$) (lower frame). The green fits are generated with the total $P(v_{net})$s in Figure 6. The blue contribution is from dissociative ionization of the stable CD_2CD_2OH radicals. The black line is the total fit. (The experimental data are reprinted with permission from Figures 9 and 11 of Womack *et al.*, J. Phys. Chem. A **116**, 6394 (2012). Copyright 2012 American Chemical Society.)

the experiment in Ref. 22. The fits on these spectra are shown in Figure 7. The fits to these two TOF spectra contain two contributions: (1) the OH/CD_2CD_2 from dissociation of the CD_2CD_2OH radicals and (2) dissociative ionization of the CD_2CD_2OH radicals. The signal from the dissociation ionization of the stable CD_2CD_2OH radicals is readily apparent in each spectrum as the sharp peak fit by the blue contribution. Womack *et al.* notes that a third contribution is also possible: the dissociation of vibrationally excited CD_2CD_2OH radicals to $CD_2H + CD_2O$. However, we do not include this in our fits because our fits are excellent without invoking that contribution. Furthermore, Rice-Ramsperger-Kassel-Marcus (RRKM) calculations[22] predict the ratio of $CD_2CD_2 + OH/CD_2H + CD_2O$ to be approximately 10 000. Table III gives the thermal fractions of the T and G precursors weighted for the fraction of radicals from each that dissociate. We used these weights without adjustment to fit to the TOF spectra. The velocity distributions predicted from our rotational dynamics calculations result in an excellent fit to the experimentally determined TOF spectra.

C. Dissociation of the 2-hydroxy-1-propyl and 1-hydroxy-2-propyl radicals to OH + propene

The dissociation of rotationally excited 2-hydroxy-1-propyl and 1-hydroxy-2-propyl radicals to OH + propene is modelled in the same manner as the dissociation of rotationally excited CD_2CD_2OH radicals to OH + ethene-d_4. The experimental work on this system photodissociated a molecular beam composed of a 70/30 mixture of 1-bromo-2-propanol and 2-bromo-1-propanol, so the system is more complex in that 17 different conformers must be considered (9 for 1-bromo-2-propanol and 8 for 2-bromo-1-propanol). The geometries and naming scheme for each of these conformers is discussed in detail in Ref. 16, but a very brief description will be given here.

The conformers differing only in the position of the hydrogen on the hydroxyl group are collected into groups. 1-bromo-2-propanol has three groups: 1TG, 1G′T, and 1GG′. The number 1 represents the carbon to which the bromine is bonded. The two letters represent the *trans* (T), *gauche clockwise* (G), and *gauche counterclockwise* (G′) designations of the Br–C–C–OH and Br–C–C–CH_3 dihedral angles, respectively, on the center carbon. Of the 2-hydroxy-1-propyl radicals resulting from 1GG′ group of conformers, only 5% have vibrational energy above the 26 kcal/mol barrier to OH + propene, so we consider only the 1TG and 1G′T groups. 2-bromo-1-propanol has three groups: 2GG′, 2TG, and 2G′T. The number 2 represents the carbon to which the bromine

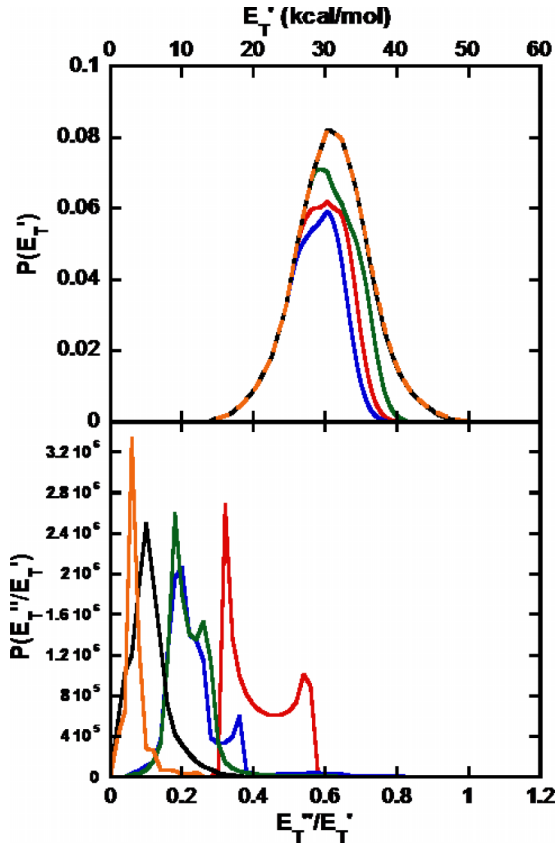

FIG. 8. (Top frame) Unstable portions of the C–Br $P(E_T)$s for the photodissociation of the 1TG (red), 1G′T (blue), 2GG′ (green), 2TG (black), and 2G′T (dashed orange) conformers of 1-bromo-2-propanol and 2-bromo-1-propanol. (Lower frame) $P\left(\frac{E_T''}{E_T'}\right)$s for the dissociation of the C_3H_6OH radicals from the 1TG conformer group (red), C_3H_6OH radicals from the 1G′T conformer group (blue), C_3H_6OH radicals from the 2GG′ conformer group (green), C_3H_6OH radicals from the 2TG conformer group (black), and C_3H_6OH radicals from the 2G′T conformer group (orange).

is bonded. The two letters represent the *trans* (T), *gauche clockwise* (G), and *gauche counterclockwise* (G′) designations of the HO–C–C–Br and HO–C–C–CH_3 group, respectively, on the center carbon.

The top frame of Figure 8 shows the portions of the total C–Br $P(E_T')$s resulting in C_3H_6OH radicals having vibrational energy above the ~26 kcal/mol barrier to OH + propene for the dissociation of each conformer group. These are used to derive the speeds of the unstable C_3H_6OH radicals. In the same manner as that discussed in Sec. III B on the dissociation of CD_2CD_2OH radicals, we present the trajectory results for the $P\left(\frac{E_T''}{E_T'}\right)$s (lower frame of Figure 8), $P(E_T'')$s (Figure 9), and the OH and propene $P(v_{net})$s for each conformer group in Figure 10 (the angular distributions are given in the supplementary material[36]). The average $\frac{E_T''}{E_T'}$ and E_T'' values are given in Table III. The photodissociation of 1-bromo-2-propanol is expected to impart large angular momenta to the 2-hydroxy-1-propyl radicals. As expected, the dissociation of the 2-hydroxy-1-propyl radicals results in OH and propene fragments with large tangential velocities. The opposite is expected for the radicals resulting from the photodissociation of 2-bromo-1-propanol, and, indeed, the

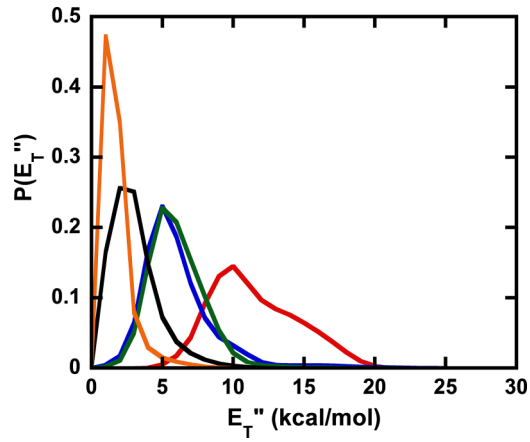

FIG. 9. $P(E_T'')$s for OH + C_3H_6 resulting from the dissociation of the C_3H_6OH radicals from the 1TG conformer group (red), C_3H_6OH radicals from the 1G′T conformer group (blue), C_3H_6OH radicals from the 2GG′ conformer group (green), C_3H_6OH radicals from the 2TG conformer group (black), and C_3H_6OH radicals from the 2G′T conformer group (orange).

trajectory calculations for the C_3H_6OH radicals from the 2TG conformer group and the C_3H_6OH radicals from the 2G′T conformer group yield OH + propene average E_T'' values only 3.1 and 1.8 kcal/mol, respectively. The C_3H_6OH radicals from

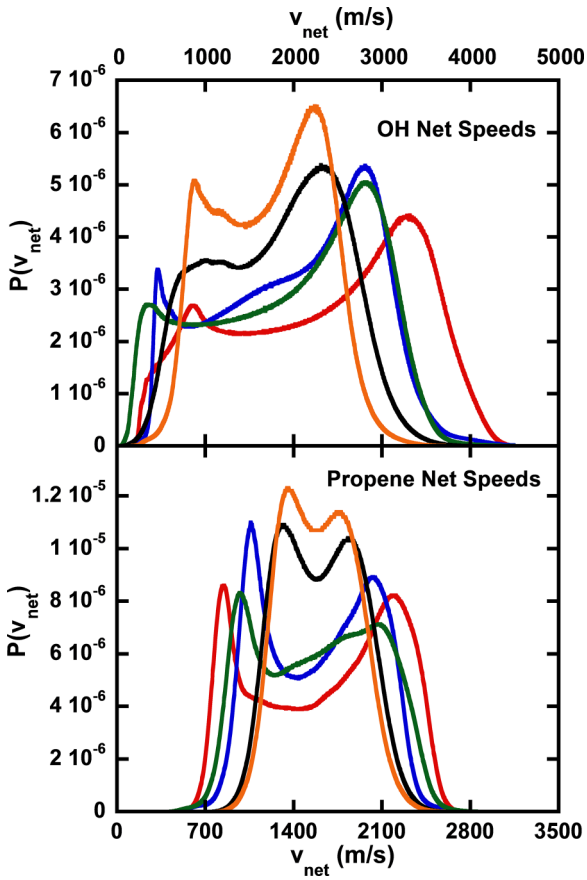

FIG. 10. $P(v_{net})$s for the OH (top frame) and propene (lower frame) fragments resulting from the dissociation of the C_3H_6OH radicals from the 1TG conformer group (red), C_3H_6OH radicals from the 1G′T conformer group (blue), C_3H_6OH radicals from the 2GG′ conformer group (green), C_3H_6OH radicals from the 2TG conformer group (black), and C_3H_6OH radicals from the 2G′T conformer group (orange).

the 2GG′ conformer group, however, have similar rotational energy to the 2-hydroxy-1-propyl radicals.

Additionally, the predicted ratios of rotational energy at the transition state to C–Br fission relative translational energy are approximately the same for both the C_3H_6OH radicals from the 1TG and 1G′T conformer groups ($\frac{E_{rot,TS}}{E'_T} \approx 0.65$). However, the average $\frac{E''_T}{E'_T}$ values for the C_3H_6OH radicals from the 1TG conformer group and C_3H_6OH radicals from the 1G′T conformer group are 0.42 and 0.24, respectively. This demonstrates the importance of determining the proper axis of rotation as it can significantly affect the tangential velocity that generates the relative velocity between the dissociation products.

Weighting and summing together the results from individual conformer groups, the total $P(v_{net})s$ for both the OH and propene fragments (Figure 11) are calculated and used to generate fits to the m/z = 42 ($C_3H_6^+$) and m/z = 17 (OH^+) experimentally determined[16] TOF spectra. These results are shown in Figure 12. Table III gives the expected and actual weightings used for the individual conformer $P(v_{net})$s. The actual weightings are in good agreement with those that were expected, with the largest deviation being ~7% for the dissociation of the C_3H_6OH radicals from the 2G′T conformer group.

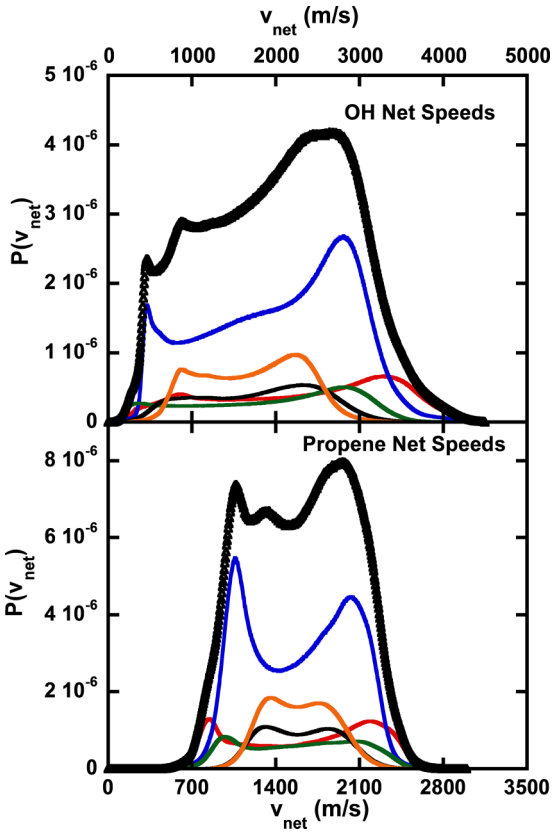

FIG. 11. Total $P(v_{net})$s (black bold line) for the OH (top frame) and propene (lower frame) fragments resulting from the dissociation of the C_3H_6OH radicals from the 1TG conformer group (red), C_3H_6OH radicals from the 1G′T conformer group (blue), C_3H_6OH radicals from the 2GG′ conformer group (green), C_3H_6OH radicals from the 2TG conformer group (black), and C_3H_6OH radicals from the 2G′T conformer group (orange), weighted by 15%, 50%, 10%, 10%, and 15%, respectively.

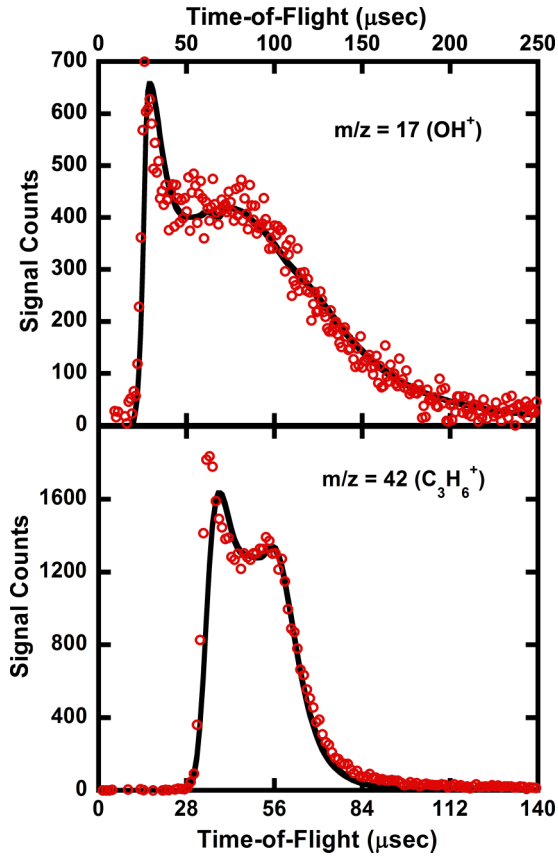

FIG. 12. TOF spectra for m/z = 17 (OH^+) (top frame) and m/z = 42 ($C_3H_6^+$) (lower frame). The black fits are generated with the total $P(v_{net})$s in Figure 11. (The experimental data are reprinted with permission from Fig. 22 of Brynteson *et al.*, J. Phys. Chem. A **118**, 3211 (2014). Copyright 2014 American Chemical Society.)

D. Comparison with quasiclassical trajectory calculations

It is interesting to compare our results to those of McKown *et al.*[24] who performed quasiclassical trajectories on a global potential energy surface to simulate the dissociation of vibrationally and rotationally excited CD_2CD_2OH radicals. In that work, quasiclassical trajectories were performed on CD_2CD_2OH radicals starting with initial conditions set to mimic those of the experimental work. We reproduce Figure 5 of Ref. 24 in Figure 13, which shows the resulting $P(E''_T)$s for two sets of initial conditions: (1) J = 0 radicals (for the sake of comparison with prior work) and (2) J = 127 a.u. (corresponding to $E'_T = 29$ kcal/mol) for the CD_2CD_2OH radicals resulting from photodissociation of the Tt conformer of 2-bromoethanol-d_4. By comparison, our predicted $P\left(\frac{E''_T}{E'_T}\right)$ shown by the solid black line in the lower frame of Figure 1 for the dissociation of the CD_2CD_2OH radicals from the T conformer group shows a very sharp distribution centered at 0.28. For photodissociations of the T conformer group of 2-bromoethanol resulting in $E'_T = 29$ kcal/mol, J = 127 a.u., our model predicts a narrow $P(E''_T)$ centered at 8 kcal/mol, shown as the dashed black distribution in Figure 14. It lies close to the peak of the $P(E''_T)$ predicted by the quasiclassical trajectory calculations. Our model only predicts velocity from the rotational motion of the radicals, so radicals with J = 0

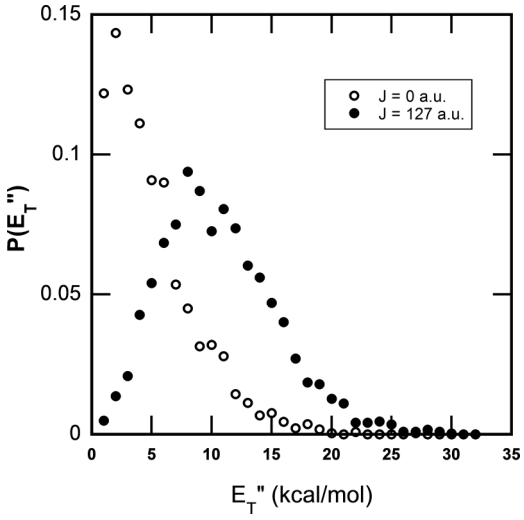

FIG. 13. Quasiclassical trajectory results for the $P(E_T'')$ for $CD_2CD_2OH \rightarrow OH + CD_2CD_2$ with the CD_2CD_2OH radicals produced from the Tt conformer of the photolytic precursor. Open circles show the prediction for the dissociation of J = 0 a.u. radicals. Filled circles show the prediction using the most probable value of J, J = 127 a.u., determined from the unstable portion of the experimentally measured C–Br photofission $P(E_T)$. Reprinted with permission from Fig. 5 of McKown *et al.*, J. Phys. Chem. A **117**, 10951 (2013). Copyright 2013 American Chemical Society.

are predicted to dissociate with $E_T'' = 0$. Of course, there are other sources of recoil kinetic energy, so the J = 0 $P(E_T'')$ presented by McKown *et al.* yields dissociations having an average E_T'' of approximately 5 kcal/mol with the largest E_T'' at 15 kcal/mol. This is broader than what one might expect from RRKM theory, so it is possible that the J = 0 $P(E_T'')$ is a result of vibrational motion either in the C–C–O bend or in the C–O stretch of the CD_2CD_2OH radical.

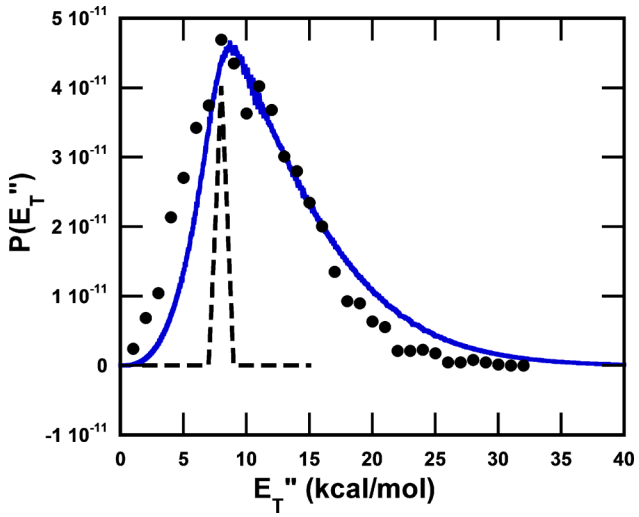

FIG. 14. $P(E_T'')$s for the dissociation of the CD_2CD_2OH radicals from the Tt conformer of 2-bromoethanol with J = 127 a.u. The distribution shown by the black circles is the result from the trajectories run by McKown *et al.* (Ref. 24). The blue distribution results convolving the speeds generated from the dashed black distribution over the speeds generated by the McKown's J = 0 $P(E_T'')$ (Figure 13) using the blue angular distribution Figure 15. (The results from the classical trajectory calculations are reprinted with permission from Fig. 5 of McKown *et al.*, J. Phys. Chem. A **117**, 10951 (2013). Copyright 2013 American Chemical Society.)

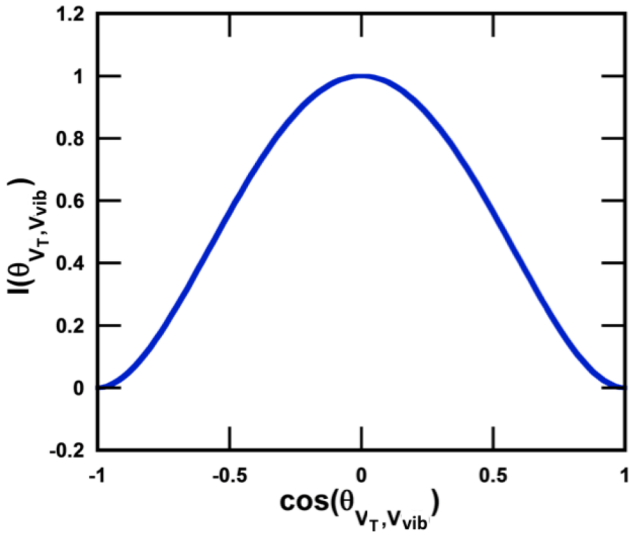

FIG. 15. A guess for the distributions of angles between the tangential velocity vector and the bending and stretching mode velocity vectors in the C–C–O plane. This angular distribution is used to derive the blue $P(E_T)$ in Figure 14.

We investigated the possibility of J = 127 a.u. radicals yielding OH + CD_2CD_2 with non-zero recoil velocity due to bending and stretching modes. The C–C–O bending mode would likely result in additional velocity vectors closely aligned or anti-aligned with the tangential velocity vector from rotation while the C–O stretch would result in additional velocity vectors mostly perpendicular to the tangential velocity vectors. We convolve our predicted OH speeds (determined from the $P(E_T'')$ shown as the black dashed line in Figure 14) over the speeds determined from McKown *et al.*'s J = 0 $P(E_T'')$ (assuming that it captures the dynamics not resulting from rotational motion) with the blue angular distribution in Figure 15, $I(\theta_{v_T,v_{vib}})$ where $\theta_{v_T,v_{vib}}$ is the angle between the tangential velocity vector and the velocity vector resulting from the bending or stretching mode. Consider now that the angular distribution that generates the best prediction for McKown's J = 127 $P(E_T'')$ peaks at $\cos\theta = 0$. This suggests it is likely that the C–O stretch contributes more to the additional velocity imparted to the dissociation fragments than does the C–C–O bend.

The take-home lesson here is that if our simple model predicts a very narrow range in $\vec{v}''_{rel}$ because the angular momentum vector $\vec{J}$ imparted to the radicals that dissociate is close to a principal axis of inertia, then one must consider the potential broadening of the recoil kinetic energy distribution by the usual energy partitioning that determines the recoil kinetic energy between the fragments from J = 0 radicals. If instead the distribution of $\vec{v}''_{rel}$ from our model is broad, as for radicals produced from the G conformers of 2-bromoethanol-d_4, these other sources of recoil velocity between the fragments are negligible in comparison.

IV. DISCUSSION

The model presented in this work predicts the net speeds of products resulting from the tangential velocity inherent

in the dissociation of rotationally excited radicals. This method first calculates the angular momenta imparted to the radicals upon photodissociation of a halogenated precursor using the measured recoil velocities in the photodissociation and assuming the rotation is imparted impulsively at the equilibrium geometry of the precursor. Subtracting the resulting E_{rot} from the internal energy of the radical identifies the unstable radical portion of the total C–Br $P(E'_T)$ for the photodissociation of each precursor conformer group, yielding the speed distributions of the radicals having sufficient vibrational energy to surmount the ~26 kcal/mol barrier to dissociation. Trajectory calculations are then performed which use the angular momentum of the radical to predict the range of tangential velocities of the dissociation products as well as the distribution of angles between the radical's velocity vector and the velocity vector of the products of the dissociation. Rather than adjusting and altering the speed distribution and angular distribution for best fit to the data, this method predicts the respective distributions with no additional alteration to these distributions.

The only adjustable parameter employed in this method to achieve a good fit is the relative weightings for the net speed distributions resulting from each conformer group. The relative weightings used to attain the best fit to the data for the dissociations studied here agree remarkably well with the predictions (see Table III). Additionally, it is seen that the contributions from each conformer group (Figure 10) yield distributions having different ranges and peaking at different speeds. Therefore, small changes in the contribution percentage from each conformer group result in noticeably poorer fits to the TOF spectra. We show these fits in the supplementary material[36] in Sec. XIV by varying the contributions from various conformer groups by 5%. These results illustrate and emphasize the marked differences in the OH + ethene-d_4/propene relative speeds as a function of the CD_2CD_2OH/C_3H_6OH angular momenta.

One of the major goals in the previously mentioned photodissociation experiments is the measurement of the product branching ratios for each dissociation channel of the radical and comparison with RRKM theory. However, to correctly compare the product branching results in these experiments to RRKM rate constants, the vibrational energy distribution and corresponding J distribution of the generated radicals must be known. In bulk kinetics experiments, typically, a thermal rotational energy is used in the RRKM calculations; however, in collision free conditions, a well-defined J distribution is necessary. Previous RRKM calculations[38] on the dissociation channels of CD_2CD_2OH used J = 4 in calculating RRKM branching ratios to compare to experiment (202-215 nm photodissociation of 2-bromoethanol-d_4). While incorporating angular momentum into the RRKM calculations is necessary, the choice of J = 4 far underestimated the average J (127 for the T conformer of the precursor) and does not correctly represent the breadth of the distribution of angular momenta of the system. Additionally, the RRKM branching results for the D atom loss channel at varying J values (4–100) demonstrated the change in product branching for the vinyl + D and acetaldehyde + D channels as J increases, expressing the importance of requiring an accurate J distribution for the system. Therefore, to adequately compare experimental branching ratios (where the radicals are photolytically generated in collision free conditions with considerable rotational energy) to RRKM branching ratios, a well-defined J distribution is necessary. As shown by the results presented in this paper, it is also imperative to consider the direction of J with respect to the principal axes, as it can significantly affect the tumbling and precession of the angular velocity vector. In conclusion, we present a simple physical model that predicts the range of tangential velocities imparted to OH + CD_2CD_2/C_3H_6OH fragments upon the dissociation of rotationally excited radicals. The results allow us to test our prediction of the angular momentum imparted to radicals during an impulsive photodissociation process. The angular momenta determined using this method predicted the speed distribution of stable radicals in prior work, and here, the predicted angular momenta have been successfully used to generate speed distributions of the unimolecular dissociation fragments. Additionally, most crossed laser-molecular beam TOF experimental work uses TOF spectra to derive, via a forward convolution fitting procedure, heavily averaged $P(E''_T)$s and $I\left(\theta_{v'_R,v''}\right)$s for the unimolecular dissociation of radicals. In this work, those two distributions are predicted, and the predicted net speed distributions generate excellent fits to the experimentally determined TOF spectra. These results also demonstrate the unfavorable consequences of using a single $P(E'_T)$ and $P(E''_T)$ when characterizing the dissociation dynamics of rotationally excited fragments; the important $\vec{J}$-dependent dynamics are obscured unless one uses a model, like the one presented here, that correctly accounts for the correlation between E'_T and E''_T.

ACKNOWLEDGMENTS

This work was supported by the Chemical Sciences, Geosciences and Biosciences Division, Office of Basic Energy Sciences, Office of Science, U.S. Department of Energy, under Grant No. DE-FG02-92ER14305 and by the National Science Foundation under Grant No. CHE-1152043.

[1]D. A. Blank, W. Sun, A. G. Suits, Y. T. Lee, S. W. North, and G. E. Hall, J. Chem. Phys. **108**, 5414 (1998).
[2]J. A. Mueller, J. L. Miller, L. J. Butler, F. Qi, O. Sorkhabi, and A. G. Suits, J. Phys. Chem. A **104**, 11261 (2000).
[3]N. Hansen, A. M. Wodtke, S. J. Goncher, J. C. Robinson, N. E. Sveum, and D. M. Neumark, J. Chem. Phys. **123**, 104305 (2005).
[4]M. L. Morton, L. J. Butler, T. A. Stephenson, and F. Qi, J. Chem. Phys. **116**, 2763 (2002).
[5]D. E. Szpunar, M. L. Morton, L. J. Butler, and P. M. Regan, J. Phys. Chem. B **106**, 8086 (2002).
[6]D. E. Szpunar, Y. Liu, M. J. McCullagh, and L. J. Butler, J. Chem. Phys. **119**, 5078 (2003).
[7]J. L. Miller, L. R. McCunn, M. J. Krisch, L. J. Butler, and J. Shu, J. Chem. Phys. **121**, 1830 (2004).
[8]K. E. Holdy, L. C. Klotz, and K. R. Wilson, J. Chem. Phys. **52**, 4588 (1970).
[9]G. E. Busch and K. R. Wilson, J. Chem. Phys. **56**, 3626 (1972).
[10]A. F. Tuck, J. Chem. Soc. Faraday Trans. **2**(73), 689 (1977).
[11]H. B. Levene, J.-C. Nieh, and J. J. Valentini, J. Chem. Phys. **87**, 2583 (1987).
[12]S. W. North, D. A. Blank, J. D. Gezelter, C. A. Longfellow, and Y. T. Lee, J. Chem. Phys. **102**, 4447 (1995).
[13]Y. Liu and L. J. Butler, J. Chem. Phys. **121**, 11016 (2004).
[14]B. J. Ratliff, C. C. Womack, X. N. Tang, W. M. Landau, L. J. Butler, and D. E. Szpunar, J. Phys. Chem. A **114**, 4934 (2010).

[15]C. C. Womack, R. S. Booth, M. D. Brynteson, L. J. Butler, and D. E. Szpunar, J. Phys. Chem. A **115**, 14559 (2011).
[16]M. D. Brynteson, C. C. Womack, R. S. Booth, S.-H. Lee, J. J. Lin, and L. J. Butler, J. Phys. Chem. A **118**, 3211 (2014).
[17]CMLAB2, version 6/93, modified by J. D. Myers. This is an interactive version built on the original cmlab program, X. Zhao, Ph.D. dissertation, University of California, 1988.
[18]B. W. Alligood, D. B. Straus, and L. J. Butler, J. Chem. Phys. **135**, 034302 (2011).
[19]D. B. Straus, L. M. Butler, B. W. Alligood, and L. J. Butler, J. Phys. Chem. A **117**, 7102 (2013).
[20]E. J. Hintsa, X. Zhao, and Y. T. Lee, J. Chem. Phys. **92**, 2280 (1990).
[21]B. J. Ratliff, B. W. Alligood, L. J. Butler, S. H. Lee, and J. J. Lin, J. Phys. Chem. A **115**, 9097 (2011).
[22]C. C. Womack, B. J. Ratliff, L. J. Butler, S.-H. Lee, and J. J. Lin, J. Phys. Chem. A **116**, 6394 (2012).
[23]E. Kamarchik, L. Koziol, H. Reisler, J. M. Bowman, and A. I. Krylov, J. Phys. Chem. Lett. **1**, 3058 (2010).
[24]B. G. McKown, M. Ceriotti, C. C. Womack, E. Kamarchik, L. J. Butler, and J. M. Bowman, J. Phys. Chem. A **117**, 10951 (2013).
[25]H. Hippler and B. Viskolcz, Phys. Chem. Chem. Phys. **2**, 3591 (2000).
[26]J. P. Senosiain, S. J. Klippenstein, and J. A. Miller, J. Phys. Chem. A **110**, 6960 (2006).
[27]R. S. Zhu, J. Park, and M. C. Lin, Chem. Phys. Lett. **408**, 25 (2005).
[28]C. Sosa and H. B. Schlegel, J. Am. Chem. Soc. **109**, 7007 (1987).
[29]C. Sosa and H. B. Schlegel, J. Am. Chem. Soc. **109**, 4193 (1987).
[30]T. Yamada, J. W. Bozzelli, and T. Lay, J. Phys. Chem. A **103**, 7646 (1999).
[31]N. K. Srinivasan, M. C. Su, and J. V. Michael, Phys. Chem. Chem. Phys. **9**, 4155 (2007).
[32]J. Zador, A. W. Jasper, and J. A. Miller, Phys. Chem. Chem. Phys. **11**, 11040 (2009).
[33]L. K. Hunh, H. R. Zhang, S. Zhang, E. Eddings, A. Sarofim, M. E. Law, P. R. Westmoreland, and T. N. Truong, J. Phys. Chem. A **113**, 3177 (2009).
[34]C. Zhou, Z. Li, and X. Li, J. Phys. Chem. A **113**, 2372 (2009).
[35]M. Szori, C. Fittschen, I. G. Csizmadia, and B. Viskolcz, J. Chem. Theory Comput. **2**, 1575 (2006).
[36]See supplementary material at http://dx.doi.org/10.1063/1.4905776 for the code which models the rotational trajectory, plots of the angle between the angular momentum and angular velocity vectors as a function of trajectory point, the trajectory results which use different numbers of transition state rotations and transition state geometries, fits to the m/z = 42 and m/z = 17 time-of-flight spectra using different conformer group weightings, and the coordinates for the principal axes and angular momentum unit vector directions used to generate Figure 2.
[37]C. C. Womack, W. H. Fang, D. B. Straus, and L. J. Butler, J. Phys. Chem. A **114**, 13005 (2010).
[38]L. W. Edwards, M. Ryazanov, H. Reisler, and S. J. Klippenstein, J. Phys. Chem. A **114**, 5453 (2010).